Ultrastrong-coupling regime of nondipolar light-matter interactions

Simone Felicetti,[1] Myung-Joong Hwang,[2] and Alexandre Le Boité[1]

[1]*Laboratoire Matériaux et Phénomènes Quantiques, Université Paris Diderot-Paris 7 and CNRS,*
10 rue Alice Domon et Léonie Duquet, 75205 Paris Cedex 13, France
[2]*Insitut für Theoretische Physik and IQST, Albert-Einstein-Allee 11, Universität Ulm, D-89069 Ulm, Germany*

We present a circuit-QED scheme which makes it possible to reach the ultrastrong-coupling regime of a nondipolar interaction between a single qubit and a quantum resonator. We show that the system Hamiltonian is well approximated by a two-photon quantum Rabi model and propose a simple scattering experiment to probe its fundamental properties. In particular, we identify a driving scheme that reveals the change in selection rules characterizing the breakdown of the rotating-wave approximation and the transition from strong to ultrastrong two-photon interactions. Finally, we show that a frequency crowding in a narrow spectral region is observable in the output fluorescence spectrum as the coupling strength approaches the collapse point, paving the way to the direct observation of the onset of the spectral collapse in a solid-state device.

I. INTRODUCTION

In cavity quantum electrodynamics (QED), the interaction between photons and atoms is often described within the dipolar approximation [1], leading to linear (single-photon) interaction terms, as exemplified by the celebrated Jaynes-Cummings and quantum Rabi models. Within this framework, considerable efforts have been made in the last decades to control and increase the light-matter coupling strength in various cavity QED experiments. The strong-coupling regime where the coupling strength is larger than any dissipation rate has been demonstrated in atomic cavity QED [2], semiconductor nanostructures [3,4], and superconducting circuits [5,6], leading to the observation of genuine quantum effects such as sub-Poissonian photon statistics [7–11]. More recent progress has also made it possible to reach the so-called ultrastrong-coupling (USC) regime where the coupling strength becomes comparable or even larger than the cavity frequency [12–21].

In this context, two-photon interaction processes (e.g., processes involving the simultaneous creation of one atomic excitation and absorption of two cavity photons) have so far been realized using second- or higher-order effects of the dipolar interaction in driven systems and therefore limited to extremely small coupling strengths [22,23]. A variety of novel physical phenomena emerges when the two-photon interaction (TPI) reaches the ultrastrong-coupling regime. In particular, a collapse of the discrete energy spectrum into a continuous band has been predicted in the ultrastrong-coupling regime of various two-photon generalizations of the quantum Rabi model (QRM) [24–28]. In the many-body limit, the TPI leads to a rich interplay between the spectral collapse and the superradiant phase transition [29,30]. However, it is an open question whether such a counterintuitive mathematical property is experimentally observable.

These considerations prompted various efforts to design quantum simulators of TPI models in different atomic platforms [31–33]. However, the implementation of a genuine TPI, where the coupling is not mediated by an external drive, requires an interaction more complex than dipolar. As recently shown, superconducting qubits coupled to microwave resonators offer a promising platform for the design of such nondipolar interactions [34,35].

In this work, we show that fundamental quantum optical phenomena due to an ultrastrong nondipolar light-matter interaction can be observed with current circuit-QED technology. To this end, we propose and analyze a device that realizes the two-photon quantum Rabi model in the nonperturbative USC regime. We characterize the circuit response under coherent driving for increasing values of the coupling strength of the genuine TPI. The transition from strong to ultrastrong nondipolar coupling is witnessed by the appearance of additional peaks in the fluorescence spectrum resulting from a change in selection rules due to the breakdown of the rotating-wave approximation. In addition, higher-order photon correlations reveal the abrupt disappearance of nonlinear effects such as the two-photon blockade for specific coupling strengths in the USC regime. Finally we show that the output field bears a clear signature of the spectral collapse.

This paper is organized as follows. In Sec. II we present the design of a nondipolar circuit QED scheme and we derive a quantum-optical model. In Sec. III we derive an input-output theory valid for all interaction regimes and we analyze the quantum-optical properties of the proposed system. Finally in Sec. IV we provide conclusive remarks and discuss the perspectives opened by our proposal.

II. CIRCUIT SCHEME

The proposed circuit is shown in Fig. 1(a). It is composed of a flux qubit and a superconducting quantum interference device (SQUID), galvanically coupled through a small inductance L. The SQUID is operated in the linear regime and, at relevant energy scales, it supports a single quantum harmonic mode. In the following we show that the nonlinear coupling
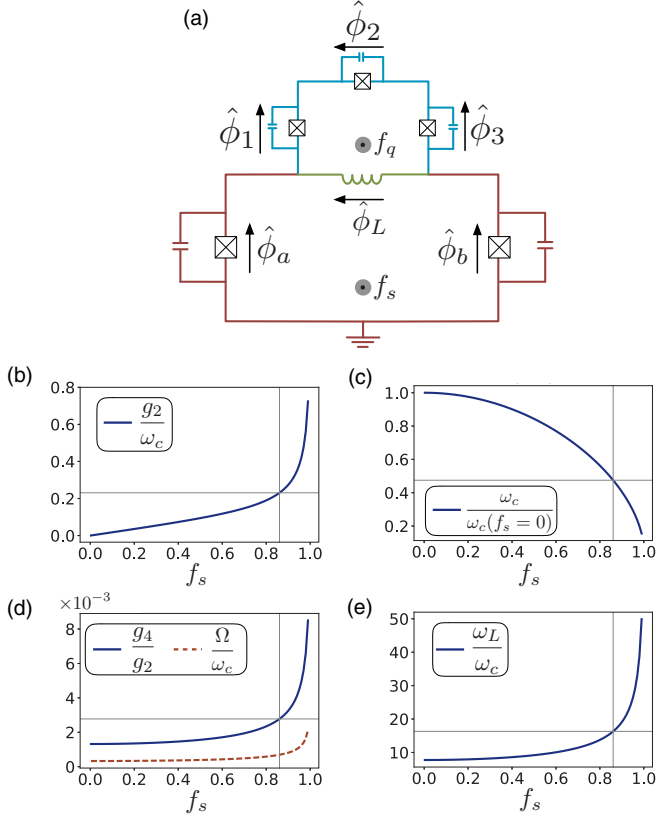
FIG. 1. (a) Sketch of the circuit scheme, a flux qubit (cyan) and a SQUID (red) galvanically coupled through a linear inductive element (green). Panels (b)–(e) show an analysis of the system's physical parameters as a function of the SQUID-loop flux bias. Straight gray lines pinpoint the values of parameters for $g_2/\omega_c = 0.23$. For the SQUID and coupling inductance we have set $E_C = 2 \times 10^{-3} E_J$ and $E_L = 30 E_J$. The flux qubit parameters have been chosen in order to meet the two-photon resonance condition $\omega_q = 2\omega_c$. Accordingly, $\widetilde{E}_J \approx 11.6 E_J$, $\widetilde{E}_C = \widetilde{E}_J/80$, and $\alpha = 0.8$.

mediated by the coupling inductance is well approximated by a TPI between the qubit and the resonator mode. More details on the derivation of the circuit model can be found in Appendix A. We divide the total circuit Lagrangian into three terms: $\mathcal{L} = \mathcal{L}_{\text{SQUID}} + \mathcal{L}_{\text{FQ}} + \mathcal{L}_L$. By applying the flux-quantization rule, the SQUID Lagrangian can be written as

$$\mathcal{L}_{\text{SQUID}} = C\dot{\phi}_+^2 + 2E_J \cos\left(\frac{\varphi_L + f_s}{2}\right) \cos(\varphi_+), \quad (1)$$

where we defined the symmetric variable $\varphi_+ = \frac{\varphi_a + \varphi_b}{2}$. The SQUID Josephson junctions have the same Josephson energy E_J and they are shunted by a capacitance C. Here and in the following, $\varphi_i = \phi_i/\phi_0$ is the gauge-invariant phase of the junction i. We also introduced the superconducting phase difference φ_L across the coupling inductance, the reduced magnetic flux quantum $\phi_0 = \hbar/2e$, and the frustration $f_s = \phi_s^{\text{ext}}/\phi_0$ due to a constant magnetic flux threading the SQUID loop. The term $\mathcal{L}_{\text{FQ}}$ is the standard Lagrangian of a flux qubit [36,37], with a modified magnetic bias. The corresponding inductive potential is given by

$$U = -2\widetilde{E}_J \cos(\varphi_p) \cos(\varphi_m) - \alpha\widetilde{E}_J \cos(2\varphi_m + f), \quad (2)$$

where $\widetilde{E}_J$ is the Josephson energy of the junctions forming the flux qubit, and α is a dimensionless parameter that renormalizes the parameters of the second junction [37]. We have also defined the flux-qubit symmetric and antisymmetric variables $\phi_p = \frac{\phi_1 + \phi_3}{2}$ and $\phi_m = \frac{\phi_1 - \phi_3}{2}$. The frustration $f = \varphi_L + f_q$ is the sum of the constant contribution $f_q = \phi_q^{\text{ext}}/\phi_0$ due to the flux flowing through the qubit loop and the coupling-inductance phase variable φ_L. Finally, the Lagrangian of the coupling inductance is $\mathcal{L}_L = \frac{C + 2\alpha\widetilde{C}}{4}\dot{\phi}_L^2 - \frac{\phi_L^2}{2L}$, which corresponds to an LC resonator of frequency $\omega_L = \sqrt{\frac{2}{L(C + \alpha\widetilde{C})}}$. Notice that in practical implementations the coupling inductance could be replaced by a Josephson junction operated in the linear regime [15]. The small correction $\widetilde{C}$ is due to the capacitance of the qubit junctions. Direct inductive coupling between the SQUID and the flux qubit is negligible for typical qubit loop dimensions.

In the following we take a perturbative approach considering the coupling inductance L as a small parameter. Accordingly, we perform two approximations: we linearize the Lagrangian with respect to the coupling-inductance phase variable ϕ_L, and then we eliminate the corresponding degree of freedom with a Born-Oppenheimer approximation. To simplify the expressions, let us define the constants $K = 2E_J \cos\left(\frac{f_s}{2}\right)$ and $S = E_J \sin\left(\frac{f_s}{2}\right)$ and the variable $\Sigma_m = \alpha\widetilde{E}_J \sin(2\varphi_m + f_q)$. First, we Taylor-expand Eqs. (1) and (2) up to first order in ϕ_L. We then take the coupling inductance L to be a small parameter and we adiabatically eliminate ϕ_L (see Appendix A). Accordingly, we assume that ω_L is much larger than the relevant system frequencies and that $\dot{\phi}_L = 0$. The Euler equation $\partial\mathcal{L}/\partial\phi_L = 0$ then results in $\phi_L = -\frac{L}{\phi_0}S \cos(\varphi_+) - \frac{L}{\phi_0}\Sigma_m$. The system Hamiltonian can be derived by defining the conjugate variables $p_i = \partial\mathcal{L}_{\text{TOT}}/\partial\dot{\varphi}_i$ and implementing the corresponding Legendre transformation. Finally, we replace the classical conjugate variables with quantum-mechanical operators $p_i \rightarrow \hat{p}_i$ and $\varphi_i \rightarrow \hat{\varphi}_i$, such that $[\hat{\varphi}_i, \hat{p}_i] = i\hbar$.

Let us discuss the different Hamiltonian terms resulting from this derivation. In $\hat{H}_0$ we gather all noninteracting terms that depend on the SQUID phase variable:

$$\hat{H}_0 = \frac{1}{4\phi_0^2 C}\hat{p}_+^2 - K\cos(\hat{\varphi}_+) - \frac{S^2}{4E_L}\cos(\hat{\varphi}_+)^2. \quad (3)$$

We assume now that the phase of the SQUID junctions is small compared to the magnetic flux quantum $\phi_+/\phi_0 \ll 1$. This approximation is valid in the limit of large Josephson energy $E_J \gg E_C = e^2/(2C)$. Accordingly, we expand the cosine functions depending on the phase variable $\hat{\varphi}_+$, neglecting terms of the order of $\hat{\varphi}_+^4$. Under this approximation the SQUID Hamiltonian is that of a quantum harmonic oscillator $\hat{H}_0 = \hbar\omega_c \hat{a}^\dagger \hat{a}$, where the creation and annihilation operators are defined as $\hat{\varphi}_+ = \sqrt{\frac{\hbar\omega_c L_{\text{eff}}}{2\phi_0^2}}(\hat{a}^\dagger + \hat{a})$ and $\hat{p}_+ = i\sqrt{\frac{\hbar\phi_0^2}{2\omega_c L_{\text{eff}}}}(\hat{a}^\dagger - \hat{a})$. The frequency of this bosonic mode is given by $\omega_c = \sqrt{\frac{1}{2CL_{\text{eff}}}}$, where $L_{\text{eff}} = \frac{\phi_0^2}{(K + \frac{S^2}{2E_L})}$.

The qubit energy contribution is given by the standard Hamiltonian $\hat{H}_{\text{FQ}}^{\text{standard}}$ of a flux qubit [36] plus two

corrections:

$$\hat{H}_{\text{FQ}} = \hat{H}_{\text{FQ}}^{\text{standard}} - \frac{\hat{\Sigma}_m^2}{4E_L} - \frac{S}{4E_L}\hat{\Sigma}_m. \qquad (4)$$

The large anharmonicity of the flux qubit allows us to perform a two-level approximation, such that $\hat{H}_{\text{FQ}}^{\text{standard}} = \hbar\omega_{\text{FQ}}\hat{\sigma}_z$. We now assume that the flux qubit is operated at the symmetry point [36]. Hence, in the two-level subspace we can write [38] $\hat{\Sigma}_m \propto \sin(2\hat{\varphi}_m + f_q) \propto \hat{\sigma}_x$, and the first correction in Eq. (4) does not couple the qubit ground and excited states. The second correction term $\frac{S}{2E_L}\hat{\Sigma}_m$ corresponds to a rotation in the qubit basis that can be compensated by a small modification of the qubit flux bias with respect to the sweet spot $f_q/\phi_0 = 0.5$.

The interaction Hamiltonian $\hat{H}_I = \frac{S}{4E_L}\hat{\Sigma}_m\hat{\varphi}_+^2$ corresponds to a nondipolar interaction between the qubit and the resonator, which is a direct consequence of the nonlinear coupling of Eq. (1). Accordingly, the total system Hamiltonian is well approximated by the two-photon quantum Rabi model with full-quadratic coupling:

$$\hat{H}_{\text{2ph}} = \omega_c\hat{a}^\dagger\hat{a} + \frac{\omega_q}{2}\hat{\sigma}_z + g_2\hat{\sigma}_x(\hat{a}^\dagger + \hat{a})^2. \qquad (5)$$

The two-photon coupling strength is given by

$$g_2 = \frac{S}{4E_L}\sqrt{\frac{E_C}{\left(K + \frac{S^2}{2E_L}\right)}}\langle 0|\hat{\Sigma}_m|1\rangle, \qquad (6)$$

where $|0\rangle$ and $|1\rangle$ are the qubit ground and excited states, respectively.

Let us now analyze the regimes of parameters accessible with the proposed scheme. In Fig. 1, we show the dependence of the system parameters on the SQUID flux bias. The effective qubit parameters have been obtained via numerical diagonalization of the Hamiltonian of Eq. (4). As the SQUID flux bias f_s increases, the two-photon coupling strength g_2 grows, while the resonator frequency decreases. In Fig. 1(b) we show that the ratio g_2/ω_c can be brought into the nonperturbative USC regime [39], making it possible to reach the vicinity of the spectral collapse. Notice that for TPI with full-quadratic coupling [35] the collapse takes place for $g_2 = 0.25\omega_c$. We take here as a reference the coupling strength $g_2/\omega_c = 0.23$. As we see in the following, this value is sufficient to observe a clear signature of the spectral collapse. Such value can be achieved with $f_s = 0.86$, where the resonator frequency is approximatively half the value it takes when no flux bias is applied to the SQUID loop $\omega_c = 0.47\omega_c^{(f_s=0)}$.

Notice that to obtain Eq. (5) we have neglected terms of the order $\hat{\varphi}_+^4$ in the resonator energy and in the coupling Hamiltonian. In Fig. 1(d) we show the ratio between the fourth-order g_4 and the two-photon g_2 coupling parameters and the ratio between the size of the quartic correction Ω and the resonator frequency ω_c. The explicit expressions of higher-order terms can be found in Appendix A. Both corrections are 3 orders of magnitude smaller than the terms considered, until the SQUID flux bias approaches the degeneracy point. Note that, as a higher-order effect, the validity of the two-level approximation is also expected to break down at the collapse point [40]. On the other hand, the validity of the adiabatic elimination of the coupling inductance is enhanced for high values of the coupling strength, as shown in Fig. 1(e).

III. QUANTUM OPTICAL PROPERTIES

A. Fluorescence spectrum

Let us now characterize the response of the system when the cavity or the qubit is driven by a monochromatic coherent field and both are coupled to a dissipative environment. The total time-dependent Hamiltonian of the system is

$$\hat{H}(t) = \hat{H}_{\text{2ph}} + F\cos(\omega_d t)(\hat{c} + \hat{c}^\dagger), \qquad (7)$$

where F is the amplitude of the driving field, ω_d is its frequency, and $\hat{c}$ is either $\hat{a}$ (cavity driving) or $\hat{\sigma}_-$ (qubit driving).

We assume that dissipation occurs via the coupling of the system to one-dimensional waveguides, described by the following Hamiltonian:

$$H_{SB} \propto \int d\omega\sqrt{\omega}(\hat{c} - \hat{c}^\dagger)(\hat{b}_\omega - \hat{b}_\omega^\dagger), \qquad (8)$$

where $\hat{c} \in \{\hat{a}, \hat{\sigma}_-\}$ and $\hat{b}_\omega$ are annihilation operators of the waveguide modes. A Markovian master equation for the density matrix $\rho(t)$ is obtained following a microscopic derivation in the weak-coupling limit. The equation has the standard Lindblad form, with jump operators involving transitions between eigenstates of $\hat{H}_{\text{2ph}}$ [41,42]. The dissipative part reads

$$\mathcal{L}\rho = \sum_{p,q=\pm}\sum_{k,j}\Theta\left(\Delta_{jk}^{pq}\right)\left(\Gamma_{jk}^{pq} + K_{jk}^{pq}\right)\mathcal{D}\left[|\Psi_j^p\rangle\langle\Psi_k^q|\right], \qquad (9)$$

where the quantities Γ_{jk}^{pq} and K_{jk}^{pq} are the rates of transition from the dressed state $|\Psi_k^q\rangle$ to $|\Psi_j^p\rangle$ due to the atomic decay and the cavity decay, respectively. They read

$$\Gamma_{jk}^{pq} = \gamma\frac{\Delta_{jk}^{pq}}{\omega_c}\left|\langle\Psi_j^p|(\hat{a} - \hat{a}^\dagger)|\Psi_k^q\rangle\right|^2, \qquad (10)$$

$$K_{jk}^{pq} = \kappa\frac{\Delta_{jk}^{pq}}{\omega_q}\left|\langle\Psi_j^p|(\hat{\sigma}_- - \hat{\sigma}_+)|\Psi_k^q\rangle\right|^2. \qquad (11)$$

The variables $p,q \in \{+, -\}$ denote the parity of the number of photons, which is a symmetry of $\hat{H}_{\text{2ph}}$. Within a given parity subspace, the eigenstates are labeled in increasing order of the energy, $E_j^p > E_i^p$ for $j > i$. The quantity $\Theta(x)$ is a step function, i.e., $\Theta(x) = 0$ for $x \leqslant 0$ and $\Theta(x) = 1$ for $x > 0$, and $\Delta_{jk}^{pq} = E_k^q - E_j^p$. We have also introduced the notation $\mathcal{D}[\mathcal{O}] = \mathcal{O}\rho\mathcal{O}^\dagger - \frac{1}{2}(\rho\mathcal{O}^\dagger\mathcal{O} + \mathcal{O}^\dagger\mathcal{O}\rho)$. Note that the system Hamiltonian on which the derivation is based does not include the external driving. For the system parameters considered here, the driving is sufficiently weak not to change the form of the jump operators (there is no "dressing of the dressed states" by the external field).

We characterize the system through correlation functions of the output field, considering that the resonator is coupled to a one-dimensional waveguide. As shown in Ref. [42], the output field in the ultrastrong coupling is proportional to the operator $\dot{X}^+$, defined in the dressed-state basis as

$$\dot{X}^+ = \sum_{p=\pm}\sum_{k,j}\Theta\left(\Delta_{jk}^{p\bar{p}}\right)\Delta_{jk}^{p\bar{p}}|\Psi_j^p\rangle\langle\Psi_j^p|i(\hat{a}^\dagger - \hat{a})|\Psi_k^{\bar{p}}\rangle\langle\Psi_k^{\bar{p}}|.$$
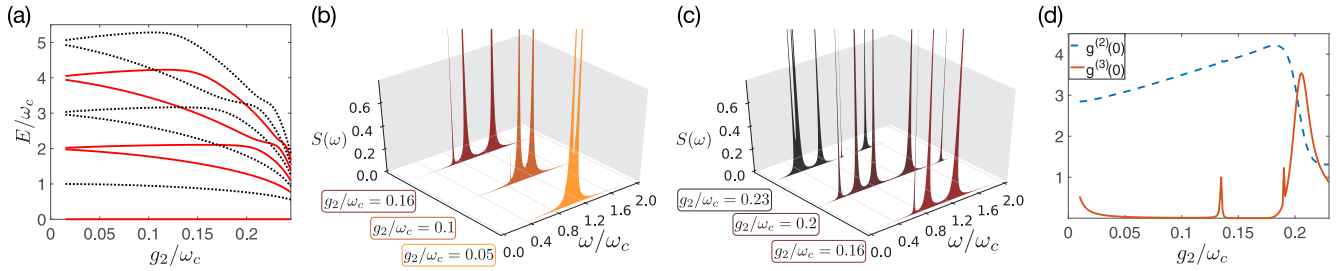
$$(12)$$

FIG. 2. (a) Energy spectrum of the two-photon Rabi Hamiltonian (without driving). Red solid lines indicate energy levels with an even number of photons while black dotted lines correspond to an odd number of photons. (b) and (c) Fluorescence spectrum in arbitrary units as a function of the coupling strength for $0.05 \leqslant g_2/\omega_c \leqslant 0.165$ in panel (b) and $0.165 \leqslant g_2/\omega_c \leqslant 0.23$ in panel (c). (d) Second- and third-order autocorrelation functions $g^{(2)}(0)$ and $g^{(3)}(0)$ as a function of g_2/ω_c. The dissipation and driving parameters are $\gamma/\omega_c = \kappa/\omega_q = 10^{-3}$ and $F/\gamma = 1$.

We first focus on the fluorescence spectrum, extracted from the two-time correlation function $g(t, t + \tau) = \langle \hat{X}^-(t)\hat{X}^+(t + \tau)\rangle$. Given the absence of a rotating frame in which the Hamiltonian is time independent, $g(t, t + \tau)$ depends both on t and τ, but it is periodic in t. The Fourier transform (relative to τ) $S(\omega, t) = \int_{-\infty}^{+\infty} d\tau e^{i\omega\tau} g(t, t + \tau)$ is then also periodic in t and the fluorescence spectrum is given by its zeroth Fourier component [43]. The function $g(t, t + \tau)$ is computed numerically by means of the quantum regression theorem [44]. In the present case, one efficient way to exploit the quantum regression theorem without performing the numerical integration of the differential equation governing $g(t, t + \tau)$ is to follow a Floquet-Liouville approach [45,46]. Within this framework, all the information about the dynamics of the system is contained in the eigvalues and eigenvector of the Floquet-Liouvillian. For the fluorescence spectrum presented in Fig. 2, we have checked that both numerical integration and diagonalization of the Floquet-Liouvillian give similar results. A derivation within the Floquet-Liouville theory is given in Appendix A.

Before discussing the numerical results, let us recall that, in addition to the parameters of the Hamiltonian, the fluorescence spectrum also depends on the particular driving scheme that we choose (i.e, on the driving frequency ω_p and the driving amplitude F/γ). In all what follows, ω_p is assumed to be resonant with the transition $|\Psi_0^+\rangle \rightarrow |\Psi_2^+\rangle$, i.e., from the ground state to the second excited state in the even-parity subspace [see the energy spectrum in Fig. 2(a)]. Note that coupling two states with the same parity is possible only when driving the qubit [$\hat{c} = \hat{\sigma}_-$ in Eq. (7)]. As we see below, this driving scheme is well suited to capture two main features of the USC regime: (i) the breaking of the selection rules and the change in symmetry due to counter-rotating terms, and (ii) the onset of the spectral collapse for $g_2/\omega_c \rightarrow 0.25$. Another important point is that the fluorescence photons that we consider result from the emission of resonator photons into the output waveguide. Therefore, as shown in Eq. (12), only the operators a and $a^\dagger$ enter in the definition of the output field, which means that only transitions changing the parity contribute to the fluorescence spectrum. In particular $|\Psi_2^+\rangle \rightarrow |\Psi_0^+\rangle$ and $|\Psi_2^+\rangle \rightarrow |\Psi_1^+\rangle$ are excluded.

Fluorescence spectrums for different values of the coupling strength, ranging from $g_2/\omega_c = 0.05$ to $g_2/\omega_c = 0.23$, are

presented in Figs. 2(b) and 2(c). For the sake of clarity they are separated into two parts. In Fig. 2(b), we observe the breaking of the selection rules and the approximate symmetry due to the rotating-wave approximation (RWA) as one enters the USC regime. For $g_2/\omega_c = 0.005$ the spectrum has only two peaks corresponding to the transitions $|\Psi_2^+\rangle \rightarrow |\Psi_0^-\rangle$ and $|\Psi_0^-\rangle \rightarrow |\Psi_0^+\rangle$, which is what we expect in the regime where the RWA is valid. Indeed, the RWA implies the conservation of the weighted excitation number $2a^\dagger a + \sigma_z$ [35] and the vanishing matrix elements $\langle\Psi_2^+|a|\Psi_1^+\rangle = \langle\Psi_2^+|\sigma_-|\Psi_1^+\rangle = 0$. This is no longer the case when one increases the coupling strength and enters the USC regime. A third resonance at the frequency of the transition $|\Psi_1^+\rangle \rightarrow |\Psi_0^-\rangle$ appears for $g_2/\omega_c = 0.1$ and $g_2/\omega = 0.165$, which means that the transition $|\Psi_2^+\rangle \rightarrow |\Psi_1^+\rangle$ is no longer forbidden by selection rules. In other words, the approximate RWA symmetry is not valid anymore and counter-rotating terms start to play an important role in the dynamics.

The structure of the fluorescence spectrum changes drastically when the coupling strength is increased further. As seen in Fig. 2(c), multiple additional peaks emerge for $g_2/\omega_c = 0.2$. This feature is related to a level crossing occurring in the energy spectrum of the two-photon QRM for $g_2 = g_\text{cross} \approx 0.17$ [see Fig. 2(a)]. For $g_2 > g_\text{cross}$, the energy of the driven state E_2^+ becomes higher than that of E_1^-, which implies that many different paths leading to the emission of output photons are now allowed when going from $|\Psi_2^+\rangle$ to the ground state. More importantly, for $g_2/\omega_c = 0.23$, the resonances appearing in the spectrum are globally red-shifted, i.e., the same number of resonances is spread over a smaller interval. The highest frequency, for example, shifts from $1.8\omega_c$ ($g_2/\omega_c = 0.2$) to $1.3\omega_c$ ($g_2/\omega_c = 0.23$). This gets more and more pronounced as the coupling strength tends to $0.25\omega_c$ and is a clear signature of the onset of the spectral collapse predicted for the two-photon QRM.

B. Two-photon blockade

The fluorescence spectrum for $g_2 < g_\text{cross}$ is also a signature of a two-photon analog of the celebrated photon blockade effect [23]. Namely, in the fluorescence spectrum for $g_2/\omega_c = 0.1$, the three resonances are the signature of two decay channels, $|\Psi_2^+\rangle \rightarrow |\Psi_0^-\rangle \rightarrow |\Psi_0^+\rangle$ and $|\Psi_2^+\rangle \rightarrow |\Psi_1^+\rangle \rightarrow |\Psi_0^-\rangle \rightarrow$

$|\Psi_0^+\rangle$. As $|\Psi_2^+\rangle \to |\Psi_1^+\rangle$ does not give rise to the emission of an output photon, these channels result in emissions of single photons or photon pairs. In addition, the anharmonicity of the spectrum ensures that no higher-order transitions are resonant with the driving frequency. More insight into this phenomenon can be gained by computing the second- and third-order autocorrelation functions of the output field defined as $g^{(2)}(0) = \langle \hat{X}^- \hat{X}^- \hat{X}^+ \hat{X}^+ \rangle / \langle \hat{X}^- \hat{X}^+ \rangle^2$ and $g^{(3)}(0) = \langle (\hat{X}^-)^3 (\hat{X}^+)^3 \rangle / \langle \hat{X}^- \hat{X}^+ \rangle^3$. The two-photon blockade is characterized by "two-photon" antibunching, i.e., the conjunction of $g^{(2)}(0) > 1$ and $g^{(3)}(0) < 1$. As shown in Fig. 2(d), we always have $g^{(2)}(0) > 1$ for the driving scheme we consider. On the other hand, $g^{(3)}(0)$ shows very rich higher-order photon correlations due to the TPI. First, focusing on the global behavior, we observe that the output field shows strong two-photon antibunching in the USC regime until $g_2 = g_{\text{cross}}$. The increase in $g^{(3)}(0)$ for $g_2 > g_{\text{cross}}$ is a direct consequence of the level crossing in the energy spectrum and the multiple decay channels available after this point. Second, it shows sharp peaks at $g_2/\omega \approx 0.13$ and $g_2/\omega \approx 0.19$. This suppression of the two-photon antibunching occurs because the energy spectrum becomes less anharmonic at these points, allowing transitions to higher-energy levels.

IV. CONCLUSIONS

In this work we have analyzed quantum optical properties of a nondipolar cavity QED system in the USC regime. First, we have proposed a superconducting quantum circuit which achieves the nonperturbative USC regime of a two-photon interaction between a single qubit and a single-mode microwave quantum resonator. Then, we have derived an input-output theory, valid in all coupling regimes, which describes the optical response of the system under coherent driving. Our analysis of the fluorescence spectrums and output field correlation functions reveals fundamental differences with respect to standard dipolar interactions.

In particular, we have proposed a driving protocol that allows one to observe fundamental features of ultrastrong two-photon couplings. First, we have shown that the appearance of an additional peak in the output fluorescence spectrum reveals the breakdown of the rotating-wave approximation. This result provides a simple method for witnessing the transition from the strong- to the ultrastrong-coupling regime of a nondipolar light-matter interaction. In addition the measurement of higher-order autocorrelation functions of the output field would exhibit a rich phenomenology, related to the successive enhancement and breakdown of the two-photon blockade effect for increasing interaction strength.

Finally, we have shown that the output fluorescence spectrum presents a clear signature of the onset of the spectral collapse. The implementation of the proposed protocol would help to solve the debate on whether the spectral collapse is only an interesting mathematical feature or a genuine physical effect with observable consequences.

ACKNOWLEDGMENTS

APPENDIX A: CIRCUIT MODEL

In this section we provide a detailed derivation of the circuit model presented in the main text.

1. Lagrangian

The system Lagrangian is given by the sum of three terms:

$$\mathcal{L}_{\text{SQUID}} = \frac{C}{2}\dot{\phi}_a^2 + \frac{C}{2}\dot{\phi}_b^2 + E_J \left[\cos\left(\frac{\phi_a}{\phi_0}\right) + \cos\left(\frac{\phi_a}{\phi_0}\right) \right],$$
(A1)

$$\mathcal{L}_{\text{FQ}} = \frac{\widetilde{C}}{2}\left[\dot{\phi}_1^2 + \dot{\phi}_3^2\right] + \frac{\alpha\widetilde{C}}{2}\dot{\phi}_2^2 + \widetilde{E}_J \left[\cos\left(\frac{\phi_1}{\phi_0}\right) + \cos\left(\frac{\phi_3}{\phi_0}\right) \right.$$
$$\left. + \alpha \cos\left(\frac{\phi_2}{\phi_0}\right) \right],$$
(A2)

$$\mathcal{L}_L = -\frac{\phi_L^2}{2L}.$$
(A3)

We define the reduced magnetic flux quantum as $\phi_0 = \Phi_0/2\pi = \hbar/2e$. We define symmetric and antisymmetric SQUID variables as $\phi_+ = \frac{\phi_a+\phi_b}{2}$ and $\phi_- = \frac{\phi_a-\phi_b}{2}$. Applying the flux-quantization rules for the SQUID loop $\phi_a - \phi_b = \phi_L + \phi_s^{\text{ext}}$, we can express the antisymmetric variable in terms of the coupling-inductance phase and the external flux flowing through the SQUID loop $\phi_- = \frac{\phi_L}{2} + \frac{\phi_s^{\text{ext}}}{2}$. Assuming a constant external flux $\dot{\phi}_s^{\text{ext}} = 0$, simple trigonometric relations allow us to rewrite the SQUID Lagrangian as

$$\mathcal{L}_{\text{SQUID}} = C\dot{\phi}_+^2 + \frac{C}{4}\dot{\phi}_L^2 + 2E_J \cos\left(\frac{\phi_L+\phi_s^{\text{ext}}}{2\phi_0}\right)\cos\left(\frac{\phi_+}{\phi_0}\right).$$
(A4)

We define symmetric and antisymmetric variables for the flux qubit as $\phi_p = \frac{\phi_1+\phi_3}{2}$ and $\phi_m = \frac{\phi_1-\phi_3}{2}$. The flux-quantization rule for the qubit loop $\phi_1 - \phi_2 - \phi_3 = -\phi_L - \phi_q^{\text{ext}}$ allows us to eliminate the phase variable of the smaller junction $\phi_2 = 2\phi_m + \phi_L + \phi_q^{\text{ext}}$. Notice that ϕ_s^{ext} is defined in the opposite direction with respect to ϕ_q^{ext}. We assume that the classical flux biasing the flux qubit is also constant, $\dot{\phi}_q^{\text{ext}} = 0$, so that

$$\mathcal{L}_{\text{FQ}} = \widetilde{C}\dot{\phi}_p^2 + \widetilde{C}\dot{\phi}_m^2 + \frac{\alpha\widetilde{C}}{2}(2\dot{\phi}_m + \dot{\phi}_L)^2$$
$$+ \widetilde{E}_J \left[2\cos\left(\frac{\phi_p}{\phi_0}\right)\cos\left(\frac{\phi_m}{\phi_0}\right) \right.$$
$$\left. + \alpha\cos\left(\frac{2\phi_m + \phi_L + \phi_q^{\text{ext}}}{\phi_0}\right) \right].$$
(A5)

Let us now detail the two main approximations performed in Sec. II, that is, the linearization of the Lagrangian with respect to the coupling-inductance phase variable ϕ_L, and the

adiabatic elimination of the corresponding degree of freedom. To simplify the expressions, we define the gauge-invariant phase variables $\varphi_i = \phi_i/\phi_0$ and the frustrations $f_s = \phi_s^{\text{ext}}/\phi_0$ and $f_q = \phi_q^{\text{ext}}/\phi_0$.

a. Linearization. We assume that the flux variable ϕ_L is small with respect to the magnetic flux quantum, and so we linearize Eq. (A4) with respect to ϕ_L:

$$\mathcal{L}_{\text{SQUID}} = C\dot{\phi}_+^2 + \frac{C}{4}\dot{\phi}_L^2 + 2E_J\left[\cos\left(\frac{f_s}{2}\right) - \sin\left(\frac{f_s}{2}\right)\frac{\varphi_L}{2}\right] \\ \times \cos(\varphi_+). \tag{A6}$$

We also linearize Eq. (A5) with respect to ϕ_L:

$$\mathcal{L}_{\text{FQ}} = \mathcal{L}_{\text{qubit}} + \frac{\alpha\widetilde{C}}{2}(\dot{\phi}_L^2 + 4\dot{\phi}_L\dot{\phi}_m)\frac{\alpha\widetilde{E}_J}{\phi_0}\sin(2\varphi_m + f_q)\phi_L, \tag{A7}$$

where with $\mathcal{L}_{\text{qubit}}$ we denote the standard Lagrangian of a flux qubit [36,37]:

$$\mathcal{L}_{\text{qubit}} = \widetilde{C}\dot{\phi}_p^2 + (1 + 2\alpha)\widetilde{C}\dot{\phi}_m^2 + E_J[2\cos(\varphi_p)\cos(\varphi_m) \\ + \alpha\cos(2\varphi_m + f_q)]. \tag{A8}$$

b. Adiabatic elimination. Let us now focus on the branch variables relative to the coupling inductance, the free Lagrangian term in $(\phi_L, \dot{\phi}_L)$ is given by

$$\mathcal{L}_{\text{coupler}} = \left(\frac{C + 2\alpha\widetilde{C}}{2}\right)\frac{\dot{\phi}_L^2}{2} - \frac{\phi_L^2}{2L}, \tag{A9}$$

which corresponds to a harmonic oscillator of frequency $\omega_L = \sqrt{\frac{2}{L(C+\alpha\widetilde{C})}}$. L being a small parameter in our development, we assume that ω_L is much larger than all other system frequencies, and we adiabatically eliminate the corresponding degree of freedom, imposing $\dot{\phi}_L = 0$. In order to simplify the expressions, in the following we make use of the following parameters:

$$K = 2E_J\cos\left(\frac{f_s}{2}\right), \quad S = E_J\sin\left(\frac{f_s}{2}\right), \tag{A10}$$

$$\Sigma_m = \alpha\widetilde{E}_J\sin(2\varphi_m + f_q). \tag{A11}$$

From Euler's equation we obtain the dependence of ϕ_L on the remaining dynamic variables:

$$\frac{\partial\mathcal{L}_{\text{TOT}}}{\partial\phi_L} = 0 \longrightarrow \phi_L = -\frac{L}{\phi_0}S\cos(\varphi_+) - \frac{L}{\phi_0}\Sigma_m. \tag{A12}$$

The total Lagrangian is obtained by adding the Eqs. (A6), (A7), and (A3), $\mathcal{L}_{\text{TOT}} = \mathcal{L}_{\text{SQUID}} + \mathcal{L}_{\text{FQ}} + \frac{\phi_L^2}{2L}$, and it can be written as

$$\mathcal{L}_{\text{TOT}} = C\dot{\phi}_+^2 + [K - S\varphi_L]\cos(\varphi_+) + \mathcal{L}_{\text{qubit}} - \Sigma_m\varphi_L \\ - \frac{\phi_0^2}{2L}\varphi_L^2. \tag{A13}$$

By replacing φ_L with Eq. (A12), we obtain finally

$$\mathcal{L}_{\text{TOT}} = C\dot{\phi}_+^2 + K\cos(\varphi_+) + \frac{S^2}{4E_L}\cos(\varphi_+)^2 \\ + \mathcal{L}_{\text{qubit}} + \frac{\Sigma_m^2}{4E_L} + \frac{S}{2E_L}\Sigma_m\cos(\varphi_+), \tag{A14}$$

where we define the inductance energy as $E_L = \phi_0^2/2L$. The first line in Eq. (A14) corresponds to the free energy terms of the SQUID, while the first two terms in the second line give the corrected bare energy of the flux qubit.

2. Hamiltonian

The system Hamiltonian can be finally derived by defining standard conjugate variables $p_i = \partial\mathcal{L}_{\text{TOT}}/\partial\dot{\varphi}_i$ and implementing the Legendre transformation. We replace now the classical variables with quantum operators and we start using the hat formalism to avoid confusion. The Hamiltonian can be written as

$$\hat{\mathcal{H}} = \hat{\mathcal{H}}_{\text{SQUID}} + \hat{\mathcal{H}}_{\text{FQ}} + \hat{\mathcal{H}}_I. \tag{A15}$$

Let us discuss the three terms independently. Using the parameters defined in Eq. (A10), the SQUID Hamiltonian is given by

$$\hat{\mathcal{H}}_{\text{SQUID}} = \frac{\hat{p}_+^2}{4C\phi_0^2} - K\cos(\hat{\varphi}_+) - \frac{S^2}{4E_L}\cos(\hat{\varphi}_+)^2. \tag{A16}$$

The Hamiltonian $\hat{\mathcal{H}}_{\text{FQ}}$ is given by the standard flux-qubit Hamiltonian, plus a correction proportional to the small parameter L:

$$\hat{\mathcal{H}}_{\text{FQ}} = \frac{\hat{p}_p^2}{4\widetilde{C}\phi_0^2} + \frac{\hat{p}_m^2}{4\widetilde{C}\phi_0^2(1 + 2\alpha)} - E_J[2\cos(\hat{\varphi}_p)\cos(\varphi_m) \\ + \alpha\cos(2\hat{\varphi}_m + fq)] - \frac{\hat{\Sigma}_m^2}{4E_L}. \tag{A17}$$

The last term in Eq. (A15) corresponds to the nondipolar coupling Hamiltonian:

$$\hat{\mathcal{H}}_I = -\frac{S}{2E_L}\hat{\Sigma}_m\cos(\hat{\varphi}_+). \tag{A18}$$

We show in the following that, in a broad regime of parameters, such nondipolar coupling can be reduced to a two-photon interaction plus an additional correction to the flux-qubit Hamiltonian.

3. Effective model

Let us now assume that the phase of the SQUID junctions is small compared to the magnetic flux quantum $\varphi_+ = \phi_+/\phi_0 \ll 1$. This approximation is valid in the limit of large Josephson energy. Expanding the cosines in Eq. (A16) we obtain

$$\hat{\mathcal{H}}_{\text{SQUID}} = \frac{\hat{p}_+^2}{4\phi_0^2C} + \left(K + \frac{S^2}{2E_L}\right)\frac{\hat{\varphi}_+^2}{2} - \left(K + \frac{2S^2}{E_L}\right)\frac{\hat{\varphi}_+^4}{24}. \tag{A19}$$

We keep orders up to $\hat{\varphi}_+^4$ and we discard constant terms. Similarly, from Eq. (A18)

$$\hat{\mathcal{H}}_I = -\frac{S}{2E_L}\hat{\Sigma}_m + \frac{S}{2E_L}\hat{\Sigma}_m\left(\frac{\hat{\varphi}_+^2}{2} - \frac{\hat{\varphi}_+^4}{24}\right), \tag{A20}$$

where the first term is a free energy term of the qubit, while the second term is the origin of the nondipolar coupling.

We now define the standard ladder operators of the quantum Harmonic oscillator corresponding to the quadratic part

of the SQUID Hamiltonian in Eq. (A19):

$$\hat{\varphi}_+ = \sqrt{\frac{\hbar \omega_c L_{\mathrm{eff}}}{2\phi_0^2}}(\hat{a}^\dagger + \hat{a}), \quad \hat{p}_+ = i\sqrt{\frac{\hbar \phi_0^2}{2\omega_c L_{\mathrm{eff}}}}(\hat{a}^\dagger - \hat{a}),$$
(A21)

where we define

$$L_{\mathrm{eff}} = \frac{\phi_0^2}{\left(K + \frac{S^2}{2E_L}\right)},$$
(A22)

$$\omega_c = \sqrt{\frac{1}{2C L_{\mathrm{eff}}}} = \frac{1}{\hbar}\sqrt{4E_C\left(K + \frac{S^2}{2E_L}\right)}, \quad (A23)$$

and where we introduce the charging energy $E_C = e^2/2C$. Equation (A19) can be then rewritten as

$$\hat{\mathcal{H}}_{\mathrm{SQUID}} = \hbar\omega \hat{a}^\dagger \hat{a} - \Omega(\hat{a}^\dagger + \hat{a})^4,$$
(A24)

where Ω is the size of the first nonlinear correction to the harmonic approximation of the SQUID Hamiltonian and reads

$$\Omega = \frac{E_C\left(K + \frac{2S^2}{E_L}\right)}{24\left(K + \frac{S^2}{2E_L}\right)}.$$
(A25)

The total qubit Hamiltonian is given by Eq. (A17) plus the free term in Eq. (A20):

$$\hat{\mathcal{H}}_{\mathrm{FQ}} = \hat{\mathcal{H}}_{\mathrm{FQ}}^{\mathrm{standard}} - \frac{\hat{\Sigma}_m^2}{4E_L} - \frac{S}{2E_L}\hat{\Sigma}_m,$$
(A26)

which corresponds to the standard Hamiltonian of a flux qubit plus two corrections. In the qubit subspace we can write $\hat{\Sigma}_m = \alpha\widetilde{E}_J\langle 0|\sin(2\hat{\varphi}_m + f_q)|1\rangle\hat{\sigma}_x = \alpha\widetilde{E}_J T(f_q)\hat{\sigma}_x$; therefore the first correction corresponds to a constant energy offset while the second one can be compensated by a small adjustment of the frustration f_q.

Finally, the second term in Eq. (A20) corresponds to the nondipolar interaction Hamiltonian between the qubit and the resonator mode:

$$\hat{\mathcal{H}}_I = g_2 \sigma_x(\hat{a}^\dagger + \hat{a})^2 + g_4 \sigma_x(\hat{a}^\dagger + \hat{a})^4,$$
(A27)

where we define the two- and four-photon coupling strengths g_2 and g_4, respectively.

$$g_2 = \frac{S}{4E_L}\sqrt{\frac{E_C}{\left(K + \frac{S^2}{2E_L}\right)}}\alpha\widetilde{E}_J T(f_q),$$
(A28)

$$g_4 = \frac{S}{48E_L}\frac{E_C}{\left(K + \frac{S^2}{2E_L}\right)}\alpha\widetilde{E}_J T(f_q).$$
(A29)

To conclude, the total system Hamiltonian up to fourth order in $\hat{\varphi}_+$ is given by the sum of Eqs. (A24), (A26), and (A27). In the main text we report the results of numerical simulations of the system Hamiltonian, showing that in a large region of physical parameters the quartic corrections Ω and g_4 are negligibly small. Accordingly, the system Hamiltonian is faithfully approximated by the two-photon quantum Rabi model. Notice that the higher-order contributions will become relevant to renormalize the spectrum of the physical model once the spectral collapse takes place.

APPENDIX B: FLUORESCENCE SPECTRUM WITHIN FLOQUET-LIOUVILLE THEORY

We derive in this section a semianalytical expression for the fluorescence spectrum within the framework of the Floquet-Liouville theory.

1. Floquet-Liouville propagator

Due to the external driving field, the total Hamlitonian is T periodic, with $T = 2\pi/\omega_d$. The Floquet-Liouville approach allows us to get rid of the explicit time dependence of the master equation by reformulating the dynamics in the space $O_p(\mathcal{H}) \otimes \mathcal{T}$, of time-periodic operators, where $\mathcal{H}$ is the underlying Hilbert space of physical states and $\mathcal{T}$ is the space of periodic functions. Using the following convention for Fourier series of periodic functions, $f(t) = \sum_{n=-\infty}^{\infty} f^{(n)}e^{-in\omega_d t}$, one can define a scalar product on $O_p(\mathcal{H}) \otimes \mathcal{T}$ as

$$\langle\!\langle A|B \rangle\!\rangle = \sum_n \mathrm{Tr}[A^{(n)\dagger}B^{(n)}],$$
(B1)

which derives from the usual scalar product on $\mathcal{T}$, $(f|g) = \frac{1}{T}\int_0^T f^*(t)g(t)dt$, and the scalar product on $O_p(\mathcal{H})$, $\langle A|B\rangle = \mathrm{Tr}[A^\dagger B]$. Within this framework the dynamics is encoded in the eigenvalues and eigenvectors of the Floquet-Liouville superoperator $\mathscr{L}$, which is time independent. For a complete derivation, see Refs. [45,46]. The central eigenvalue problem is then

$$\mathscr{L}|R_{\alpha,k}\rangle\!\rangle = \Omega_{\alpha,k}|R_{\alpha,k}\rangle\!\rangle,$$
(B2)

where $0 \leqslant \alpha \leqslant \dim(\mathcal{H})^2 - 1$ and $k \in \mathbb{Z}$. Note that the object $|R_{\alpha,k}\rangle\!\rangle$ defines a periodic matrix, i.e., for each time t, $R_{\alpha,k}(t) \in O_p(\mathcal{H})$. As $\mathscr{L}$ is not Hermitian, it is necessary to distinguish the right eigenvectors defined above from the left eigenvectors obeying

$$\mathscr{L}^\dagger|L_{\alpha,k}\rangle\!\rangle = \Omega_{\alpha,k}^*|L_{\alpha,k}\rangle\!\rangle.$$
(B3)

Using these notations, one can write a propagator for the master equation

$$\rho(t+\tau) = U(t+\tau, t)[\rho(t)]$$
$$= \sum_{\alpha,k} e^{-i\Omega_{\alpha,k}\tau}\langle\!\langle L_{\alpha,k}|\rho\rangle\!\rangle R_{\alpha,k}(t+\tau). \quad (B4)$$

2. Quantum regression theorem and fluorescence spectrum

In the ultrastrong-coupling regime, there is no rotating frame in which the Hamiltonian is time independent. As a result, the correlation function

$$g(t, t+\tau) = \langle \dot{X}^-(t)\dot{X}^+(t+\tau)\rangle$$
(B5)

depends on both t and τ. In the present context, due to the periodic driving, it is periodic in t. We can therefore define the periodic spectrum $S(\omega, t) = \int_{-\infty}^{+\infty} e^{i\omega\tau}g(t, t+\tau)$. Following the derivation of the standard Wiener-Khinchin theorem, we find that the relevant quantity is the zeroth Fourier component of $S(\omega, t)$:

$$S(\omega) = \lim_{t_0 \to \infty}\left[\frac{1}{T}\int_{t_0}^{t_0+T}\int_{-\infty}^{+\infty} e^{i\omega\tau}g(t, t+\tau)dt d\tau\right].$$
(B6)

The function in Eq. (B5) is computed by applying the quantum regression theorem. For any operators $\hat{a}$ and $\hat{b}$ and time $\tau > 0$, we have

$$\langle a(t)b(t+\tau)\rangle = \text{Tr}\{bU(t+\tau, t)[\rho(t)a]\}. \quad \text{(B7)}$$

Injecting the expression of the propagator into this last expression we find

$$\langle \dot{X}^-(t)\dot{X}^+(t+\tau)\rangle$$
$$= \sum_{\alpha,k} e^{-i\Omega_{\alpha,k}\tau}\langle\!\langle L_{\alpha,k}|\rho_\infty\dot{X}^-\rangle\!\rangle\text{Tr}[\dot{X}^+ R_{\alpha,k}(t+\tau)] \quad \text{(B8)}$$

$$= \sum_{\alpha,k,m} e^{-i(\Omega_{\alpha,k}+m\omega_d)\tau-im\omega_d t}\langle\!\langle L_{\alpha,k}|\rho_\infty\dot{X}^-\rangle\!\rangle\text{Tr}[\dot{X}^+ R_{\alpha,k}^{(m)}].$$

$$\text{(B9)}$$

Explicit calculation for $\tau < 0$ can be avoided by inverting the order of the integrals in Eq. (B6). The spectrum then reads $S(\omega) = 2\text{Re}[\int_0^\infty d\tau e^{i\omega\tau}g_+(\tau)]$, with $g_+(\tau) = \lim_{t_0\to\infty}\frac{1}{T}\int_{t_0}^{t_0+T}g(t, t+\tau)dt$. Since averaging on t selects the component $m = 0$ in Eq. (B9), we find

$$g_+(\tau) = \sum_{\alpha,k} e^{-i\Omega_{\alpha,k}\tau}\langle\!\langle\dot{X}^-, 0|R_{\alpha,k}\rangle\!\rangle\langle\!\langle L_{\alpha,k}|\rho_\infty\dot{X}^-\rangle\!\rangle. \quad \text{(B10)}$$

The final semianalytical expression for the fluorescence spectrum is then

$$S(\omega) = -2\text{Re}\left[\sum_{\alpha,k}\frac{\langle\!\langle\dot{X}^-, 0|R_{\alpha,k}\rangle\!\rangle\langle\!\langle L_{\alpha,k}|\rho_\infty\dot{X}^-\rangle\!\rangle}{i(\omega - \Omega_{\alpha,k})}\right]. \quad \text{(B11)}$$

Due to the dissipative nature of the system, the eigenvalues $\Omega_{\delta\eta,k}$ are complex and satisfy $\text{Im}[\Omega_{\alpha,k}] \leqslant 0$. If $\text{Im}[\Omega_{\alpha,k}] = 0$, the denominator has to be understood as

$$\frac{-1}{i(\omega - \Omega_{\alpha,k} + i0^+)} = \pi\delta(\omega - \Omega_{\alpha,k}) + i\text{P}\frac{1}{\omega - \Omega_{\alpha,k}}, \quad \text{(B12)}$$

where P stands for Cauchy's principal value.

[1] C. Cohen-Tannoudji, J. Dupont-Roc, and G. Grynberg, *Photons and Atoms: Introduction to Quantum Electrodynamics*, (Wiley, New York, 1989).

[2] G. Rempe, H. Walther, and N. Klein, Phys. Rev. Lett. **58**, 353 (1987).

[3] J. P. Reithmaier, G. Sek, A. Löffler, C. Hofmann, S. Kuhn, S. Reitzenstein, L. V. Keldysh, V. D. Kulakovskii, T. L. Reinecke, and A. Forchel, Nature (London) **432**, 197 (2004).

[4] E. Peter, P. Senellart, D. Martrou, A. Lemaître, J. Hours, J. M. Gérard, and J. Bloch, Phys. Rev. Lett. **95**, 067401 (2005).

[5] A. Wallraff, D. I. Schuster, A. Blais, L. Frunzio, R.- S. Huang, J. Majer, S. Kumar, S. M. Girvin, and R. J. Schoelkopf, Nature (London) **431**, 162 (2004).

[6] X. Gu, A. F. Kockum, A. Miranowicz, Y. X. Liu, and F. Nori, Phys. Rep. **718-719**, 1 (2017).

[7] A. Imamoglu, H. Schmidt, G. Woods, and M. Deutsch, Phys. Rev. Lett. **79**, 1467 (1997).

[8] K. M. Birnbaum, A. Boca, R. Miller, A. D. Boozer, T. E. Northup, and H. J. Kimble, Nature (London) **436**, 87 (2005).

[9] D. Bozyigit, C. Lang, L. Steffen, J. M. Fink, C. Eichler, M. Baur, R. Bianchetti, P. J. Leek, S. Filipp, M. P. da Silva, A. Blaisand, and A. Wallraff, Nat. Phys. **7**, 154 (2011).

[10] C. Lang, D. Bozyigit, C. Eichler, L. Steffen, J. M. Fink, A. A. Abdumalikov, Jr., M. Baur, S. Filipp, M. P. da Silva, A. Blais, and A. Wallraff, Phys. Rev. Lett. **106**, 243601 (2011).

[11] A. J. Hoffman, S. J. Srinivasan, S. Schmidt, L. Spietz, J. Aumentado, H. E. Türeci, and A. A. Houck, Phys. Rev. Lett. **107**, 053602 (2011).

[12] M. H. Devoret, S. Girvin, and R. Schoelkopf, Ann. Phys. **16**, 767 (2007).

[13] J. Bourassa, J. M. Gambetta, A. A. Abdumalikov, Jr., O. Astafiev, Y. Nakamura, and A. Blais, Phys. Rev. A **80**, 032109 (2009).

[14] Y. Todorov, A. M. Andrews, R. Colombelli, S. De Liberato, C. Ciuti, P. Klang, G. Strasser, and C. Sirtori, Phys. Rev. Lett. **105**, 196402 (2010).

[15] T. Niemczyk *et al.*, Nat. Phys. **6**, 772 (2010).

[16] P. Forn-Díaz, J. Lisenfeld, D. Marcos, J. J. García-Ripoll, E. Solano, C. J. P. M. Harmans, and J. E. Mooij, Phys. Rev. Lett. **105**, 237001 (2010).

[17] P. Nataf and C. Ciuti, Phys. Rev. Lett. **107**, 190402 (2011).

[18] P. Forn-Díaz, G. Romero, C. J. P. M. Harmans, E. Solano, and J. E. Mooij, Sci. Rep. **6**, 26720 (2016).

[19] P. Forn-Díaz, J. J. García-Ripoll, B. Peropadre, J.-L. Orgiazzi, M. A. Yurtalan, R. Belyansky, C. M. Wilson, and A. Lupascu, Nat. Phys. **13**, 39 (2017).

[20] F. Yoshihara, T. Fuse, S. Ashhab, K. Kakuyanagi, S. Saito, and K. Semba, Nat. Phys. **13**, 44 (2017).

[21] Z. Chen, Y. Wang, T. Li, L. Tian, Y. Qiu, K. Inomata, F. Yoshihara, S. Han, F. Nori, J. S. Tsai, and J. Q. You, Phys. Rev. A **96**, 012325 (2017).

[22] A. Di Piazza, C. Müller, K. Z. Hatsagortsyan, and C. H. Keitel, Rev. Mod. Phys. **84**, 1177 (2012).

[23] C. Hamsen, K. N. Tolazzi, T. Wilk, and G. Rempe, Phys. Rev. Lett. **118**, 133604 (2017).

[24] I. Travenec, Phys. Rev. A **85**, 043805 (2012).

[25] V. V. Albert, G. D. Scholes, and P. Brumer, Phys. Rev. A **84**, 042110 (2011).

[26] Q.-H. Chen, C. Wang, S. He, T. Liu, and K.-L. Wang, Phys. Rev. A **86**, 023822 (2012).

[27] L. Duan, Y.-F. Xie, D. Braak, and Q.-H. Chen, J. Phys. A: Math. Theor. **49**, 464002 (2016).

[28] S. Cui, J.-P. Cao, H. Fan, and L. Amico, J. Phys. A: Math. Theor. **50**, 204001 (2017).

[29] L. Garbe, I. L. Egusquiza, E. Solano, C. Ciuti, T. Coudreau, P. Milman, and S. Felicetti, Phys. Rev. A **95**, 053854 (2017).

[30] X.-Y. Chen and Y.-Y. Zhang, Phys. Rev. A **97**, 053821 (2018).

[31] S. Felicetti, J. S. Pedernales, I. L. Egusquiza, G. Romero, L. Lamata, D. Braak, and E. Solano, Phys. Rev. A **92**, 033817 (2015).

[32] R. Puebla, M.-J. Hwang, J. Casanova, and M. B. Plenio, Phys. Rev. A **95**, 063844 (2017).

[33] P. Schneeweiss, A. Dareau, and C. Sayrin, Phys. Rev. A **98**, 021801(R) (2018).

[34] J. Goetz, F. Deppe, K. G. Fedorov, P. Eder, M. Fischer, S. Pogorzalek, E. Xie, A. Marx, and R. Gross, Phys. Rev. Lett. **121**, 060503 (2018).

[35] S. Felicetti, D. Z. Rossatto, E. Rico, E. Solano, and P. Forn-Díaz, Phys. Rev. A **97**, 013851 (2018).

[36] T. P. Orlando, J. E. Mooij, L. Tian, C. H. van der Wal, L. S. Levitov, Seth Lloyd, and J. J. Mazo, Phys. Rev. B **60**, 15398 (1999).

[37] C. H. van der Wal, A. C. J. ter Haar, F. K. Wilhelm, R. N. Schouten, C. J. P. M. Harmans, T. P. Orlando, S. Lloyd, and J. E. Mooij, Science **290**, 773 (2000).

[38] Y. X. Liu, J. Q. You, L. F. Wei, C. P. Sun, and F. Nori, Phys. Rev. Lett. **95**, 087001 (2005).

[39] D. Z. Rossatto, C. J. Villas-Bôas, M. Sanz, and E. Solano, Phys. Rev. A **96**, 013849 (2017).

[40] D. De Bernardis, P. Pilar, T. Jaako, S. De Liberato, and P. Rabl, arXiv:1805.05339; A. Stokes and A. Nazir, arXiv:1805.06356.

[41] F. Beaudoin, J. M. Gambetta, and A. Blais, Phys. Rev. A **84**, 043832 (2011).

[42] A. Ridolfo, M. Leib, S. Savasta, and M. J. Hartmann, Phys. Rev. Lett. **109**, 193602 (2012).

[43] D. Malz and A. Nunnenkamp, Phys. Rev. A **94**, 023803 (2016).

[44] H. J. Carmichael, *Statistical Methods in Quantum Optics 1* (Springer, Berlin, 1998).

[45] T.-S. Ho, K. Wang, and Shih-I Chu, Phys. Rev. A **33**, 1798 (1986).

[46] A. Le Boité, M.-J. Hwang, and M. B. Plenio, Phys. Rev. A **95**, 023829 (2017).